Measuring Secondary Phases in Duplex Stainless Steels

I. Calliari, K. Brunelli, M. Dabalà, and E. Ramous

The use of duplex stainless steels is limited by their susceptibility to the formation of dangerous intermetallic phases resulting in detrimental effects on impact toughness and corrosion resistance. This precipitation and the quantitative determinations of the phases have received considerable attention and different precipitation sequences (σ phase, χ phase, and carbides) have been suggested. This study investigates the phase transformation during continuous cooling and isothermal treatments in commercial duplex stainless steel grades and the effects on alloy properties, and compares the most common techniques of analysis.

INTRODUCTION

A favorable combination of mechanical and corrosion properties characterizes duplex stainless steels (DSS), as they consist of almost equal parts of austenite and ferrite.[1,2] Duplex steels are more susceptible to precipitation of intermetallic phases than austenitic steels due to their high chromium and molybdenum contents and high diffusion rates in the ferrite phase. These steels are prone to form secondary phases after exposure to temperatures ranging from 450ºC to 1,000ºC.[3] The σ phase is a hard, brittle non-magnetic intermetallic phase, with high chromium and molybdenum contents, affecting both hot and room temperature ductility. Some authors report that χ phase precipitates for shorter times than σ[4] and at slightly lower temperatures, but it has not been well investigated.

These precipitates cause a dramatic deterioration in toughness and corrosion resistance.[5,6] It has been demonstrated that over a certain amount (between 5% and 10%) of a phase like σ phase, the toughness of duplex steels is reduced to values too low for practical applications, but some features of the early stages of precipitation are not yet well understood.

A very low cooling rate may determine different microstructures from surface to core, especially in large-sized bars, with a surface free of secondary phases and a core with a significant amount of them. Therefore the critical cooling rate should be determined in order to avoid or to limit precipitation at the core. As a consequence of these characteristics, the correct procedure[7,8] for measuring low contents of σ-related phases is needed, as the requirement for manufacturing or welding DSS to be "free of intermetallic phases" may be too strict. Starting from these data, it is evident that the metallographic techniques used for secondary phase identification play a fundamental role in phase identification. Efforts have been made to determine the volume fraction of σ phases in austenitic[9] stainless steel and in duplex grades. Several electrochemical procedures[10] and metallographic etchants[11] have been tested and discussed for light microscopy,[12] but it is quite difficult to identify separately χ and σ and to accurately quantify low amounts of such phases.

In this paper, the results concerning the formation of secondary phases in commercial DSS SAF 2205 and SAF 2507 are presented. The precipitation has been examined during continuous cooling (SAF 2205) and isothermal treatments (SAF 2205 and SAF 2507). The goal of this study was to investigate the sequence of precipitation in different thermal conditions and to compare the different techniques of precipitation analysis.

See the sidebar for experimental procedures.

How would you…

…describe the overall significance of this paper?

The paper improves the knowledge on the precipitation kinetics of dangerous intermetallic phases which have a detrimental effect on the toughness of duplex stainless steel. Furthermore, a comparison between different measuring techniques of analysis was performed.

…describe this work to a materials science and engineering professional with no experience in your technical specialty?

This work investigated the effect of aging temperature, time of treatments, and cooling rates on the microstructure (austenite/ferrite ratio) and the amount of secondary phase precipitation on two duplex stainless steels. This work was done to find the thermal conditions to avoid toughness depletion, which can cause premature failure of these steels.

…describe this work to a layperson?

Stainless steels, especially the grade used in this study, suffer from lower toughness caused by secondary phase precipitation especially when these steels undergo thermal treatments. In this study the influence of thermal treatment parameters on the precipitation of these secondary phases was investigated.

RESULTS AND DISCUSSION

Solution-Treated Sample

The solution-treated materials have banded structure with elongated gamma islands in the longitudinal sections, while the transverse sections have ferrite and austenite grains with isotropic structure. The values of volume frac-

tions of ferrite and austenite, measured with image analysis on an optical microscope (OM), are, respectively, austenite = 1±4% and ferrite = 49±4% in SAF 2205, and austenite 45±3% and ferrite 55±3% in SAF 2507. These are typical values for solution-annealed samples. No secondary phases were detected with scanning electron microscopy-backscattered electron microscopy (SEM-BSE).

Heat-Treated Samples

Murakami and Groesbeck

At first, the capabilities of Murakami and Groesbeck reagents were tested on a group of SAF 2205 samples. In Figures 1 and 2 the OM and SEM-BSE micrographs, taken at 1,000× of the sample treated at 850ºC for 25 min., are shown. In Figure 1, the effectiveness of Groesbeck and Murakami reagents are difficult to determine. When the secondary phases are at micrometric scale the corrosion products overestimate them. On the contrary the SEM-BSE (Figure 2) micrograph shows all the phases, and the ferrite appears darker than austenite, while the secondary phases are lighter. An SEM-BSE image at higher magnification is shown in Figure 3, in which ferrite, austenite, χ, and σ are marked. The particles of χ are brighter than σ as their molybdenum content is higher.

It may be concluded that the tested chemical etchants are not suitable to identify, or to accurately quantify secondary phases.

Electrochemical Etching

The use of NaOH for 6 s, 8 s, and 10 s results in a strong etching of the grain boundaries. The presence of secondary phases is revealed with 8 s of application but the phases are not easily distinguishable from the grain boundaries, without differences between χ and σ. The influence of immersion time is evident, with remarkable differences from 6 s (no secondary phases) to 8 s and 10 s. It can be concluded that NaOH is not suitable for secondary phases measurement, as it is too affected by the immersion time. On the contrary, the immersion in modified Nital 10 results in a good detection of secondary phases, but the grain boundaries are outlined, so it is quite difficult to identify the phases with IA. Nital 10 gives a good contrast between matrix and precipitated phases: austenite is light blue, ferrite is white and all precipitated phases are dark, without any differences between σ and χ. On the contrary in the SEM-BSE micrograph (Figure 2) χ and σ are well identified.

The immersion in NH_3 results in a strong etching of secondary phases, without any attack of grain boundaries and alloy matrix (Figure 4b). This confirms that the precipitation is mainly at grain boundaries, but no difference between χ and σ was seen. On the con-

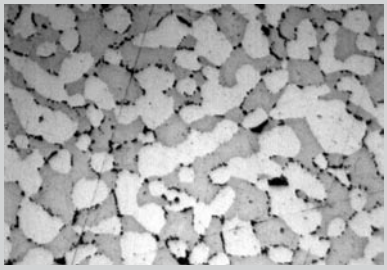

10 µm

Figure 1. An OM micrograph of a sample treated at 850°C, 25 min., after etching with Groesbeck.

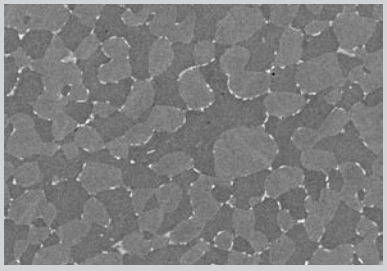

10 µm

Figure 2. An SEM-BSE micrograph of a sample treated at 850°, 25 min.

EXPERIMENTAL PROCEDURES

The as-received materials were wrought SAF 2205 and SAF 2507 rods (30 mm) in the solution-annealed condition, with compositions reported in Table A.

Isothermal aging treatments of annealed specimens were carried out at temperatures of 780–1,000ºC for times in the range of 5–120 min. Relatively short aging times were chosen so low amounts of secondary phases could be measured to investigate their precipitation kinetics. Continuous cooling tests were performed in a Setaram "Labsys TG" machine, in argon atmosphere. Samples (diameter 6 mm, length 8 mm) were solution treated for 5 min. at temperatures of 1,020ºC and 1,050ºC. The samples were then cooled in argon at various cooling rates in the range of 0.02–0.4ºC/s. The volume fractions of ferrite and austenite in solution-treated samples were measured by image analysis on light micrographs at 200×, after etching with the Beraha reagent (room temperature [R.T.], 10 s).

Different phases were identified by scanning electron microscope (SEM) examination of unetched samples, using the backscattered electron (BSE) signal, on the basis of atomic number contrast effect: the ferrite appears slightly darker than austenite, while the secondary phases are lighter. The amounts of secondary phases were determined using image analysis software on SEM-BSE micrographs (10 fields, 1,000×) and the contribution of each phase to total volume fractions was determined. The SEM operated at 25kV; the BSE detector was set to maximize the atomic number contrast, allowing ferrite, austenite, and secondary phases' identification. Scanning electron microscopy-electron dispersive spectroscopy determined the chemical composition of the phases on unetched samples. The secondary phases were also quantified with image analysis on optical micrographs after etching with different reagents. An investigation on the capabilities of the reagents named Murakami (aqueous solution of 10% $K_3Fe(CN)_6$ and 10% KOH) and Groesbeck (aqueous solution of 4% $KMnO_4$ + 4% NaOH), and an electrolytic etching (Nital and concentrated solution of NH_3, 3.5 V, R.T.) was performed by etching different samples with the same reagent and the same sample with different reagents.

Instrumented Charpy–V impact specimens, after isothermal treating, were prepared in the standard form of 10×10×55 mm^3. Impact testing was done at room temperature.

Table A. Chemical Composition (wt.%) of SAF 2205 and SAF 2507.

	C	Si	Mn	Cr	Ni	Mo	P	S	N	Cu	W	Fe
2205	0.03	0.56	1.46	22.75	5.04	3.19	0.025	0.002	0.160	—	—	bal
2507	0.03	0.43	0.54	24.48	6.36	4.0	0.020	0.008	0.263	0.67	0.72	bal

trary the phases are well discriminated in SEM-BSE image Figure 4a.

Thus, electrochemical etching with NH_3 can be considered the best method to detect secondary phases with OM, but without any distinction between χ and σ.

The capabilities of OM and SEM-BSE can be appreciated in Figure 5, where the amounts of secondary phases in the SAF 2205 as a function of holding time (temperature 900ºC) is reported. In samples with a low content of secondary phases, the corrosion products enhance the boundary effect and the immersion time affects the detection of phases. The result is that at the lowest phase's contents (<1%), the OM data differ from SEM data by about 50–100%.

Pores and inclusions that may have the same gray-scale appearance as intermetallic phases may be another potential source of errors in OM images. Moreover in SEM-BSE the pores and inclusions are dark while the secondary phases are bright. They are identified as the result of the spatial distribution of elements; the uncertainty is only related to the beam resolution. The influence of secondary phases on toughness was studied through Charpy impact tests (at room temperature) (Figure 6). An attempt has been made to correlate the toughness to volume fraction of intermetallic phases since impact toughness depends on the amount and types of intermetallic phases.

In the OM data obtained on samples etched with NH_3, the discrepancy is evident, suggesting that SEM-BSE is more accurate than OM in detecting and measuring the amount of secondary phases with image analysis. The solubilized material has average impact energy of 250 J, but only 0.5% of the secondary phases, measured on SEM micrographs, reduce it to about 100 J. A further drop occurs at 1%, when the impact energy is about 50 J, and the final severe deterioration of toughness is induced by higher values (fractions > 1.5–2%). This statement agrees with the generally accepted specification for the DSS: a phase content of less than 1% or lower to maintain the toughness value of 40–50 J.

A critical discussion of this deterioration and fracture mechanism is reported in another paper.[13] Starting from the discussed method capabilities and from the effects of secondary phase on toughness, the amounts of secondary phases have been measured in SAF 2205 and SAF 2507. A short summary[14,15] of the data is published elsewhere.

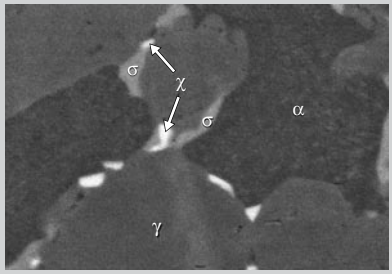

Figure 3. An SEM-BSE, high magnification image of the sample in Figure 2, with χ, σ, ferrite, and austenite.

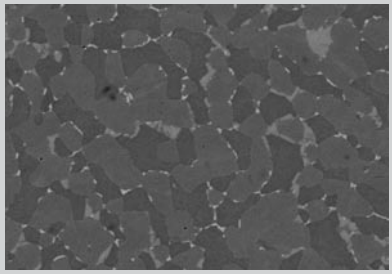

a

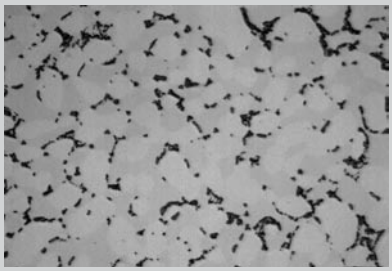

b

Figure 4. (a) An SEM-BSE micrograph (900ºC, 40 min.); (b) optical micrograph (900ºC, 40 min.).

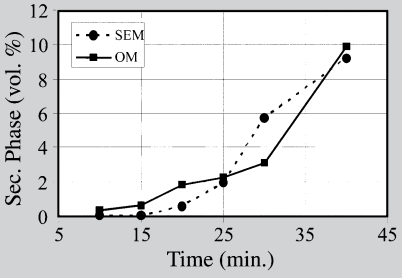

Figure 5. A match between vol. % of secondary phases measured on SEM and OM (NH_3) micrographs (heat treatment 900°C).

ISOTHERMAL TREATMENT OF SAF 2205 AND SAF 2507

Precipitation in SAF 2205

After aging at 780ºC, the first precipitates were identified as χ at high magnification (2,000–4,000x) after 1,800 s aging and become more evident after 2,400 s. The quantitative determination is not possible.

After aging at 850ºC, the χ phase appears after about 600 s, while the σ phase appears after about 20 min. After 30 min. the χ phase and the σ phase are both present: the χ phase is always at the ferrite/austenite and ferrite/ferrite boundaries. The σ phase penetrates the ferrite or grows along the ferrite/austenite boundary.

After aging at 900ºC, as at 850ºC, the first phase present is the χ phase at the grain boundaries. By increasing the

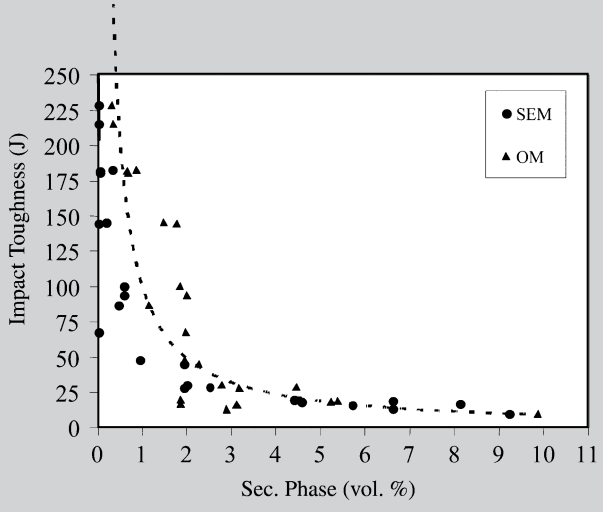

Figure 6. The impact toughness versus % vol. of secondary phases measured on optical and SEM images.

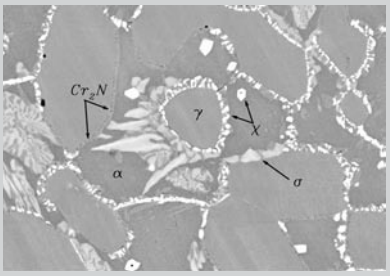

3 µm

Figure 7. An SEM-BSE micrograph of the sample treated at 900ºC for 2,400 s.

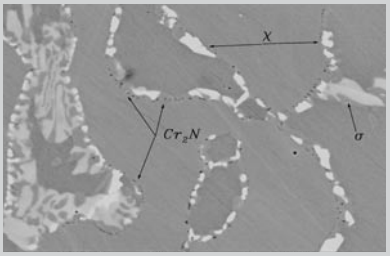

3 µm

Figure 8. An SEM-BSE micrograph of the sample treated at 950ºC for 4,800 s.

time, the amount of χ phase increases and the σ phase also appears in the form of coarser precipitates at the γ/α boundary, but growing into the ferrite. Although σ particles are, at the beginning, less numerous than the χ-phase particles, they are coarser and grow more rapidly, quickly reaching almost the same volume fraction. By increasing the holding time, the σ phase grows to large particles, moving from the boundaries into the ferrite, embedding some small χ particles. This seems to show the progressive transformation of χ phase to σ phase.

Precipitation in SAF 2507

After aging at 800ºC, no precipitation was detected. When aging at 850ºC, the first χ precipitates appear after 900 s aging and become more evident after 1,200 s at boundaries and sometimes inside the ferrite grains. No σ phase has been detected. The small size and very low amount of the particle do not allow measurement of the volume fractions, which can be reasonably estimated to be less than 0.1%.

After aging at 900ºC, the χ phase appears after about 300 s at grain boundaries, with some isolated σ-phase particles. A few small dark precipitates were detected at grain boundaries, identified as Cr_2N on the basis of N peaks. After 2,400 s χ, σ, and nitrides are present: χ phase is always at the ferrite/austenite and ferrite/ferrite boundaries (Figure 7). At this temperature the formation kinetic of χ phase is favored.

After aging at 950ºC, the first precipitates of χ appear after 180 s, while σ appears after 300 s. The percentage of σ phase increases with time, while the percentage of χ phase decreases after 1,800 s. Although σ particles are, at the beginning, less numerous than χ-phase particles, they are coarser and grow more rapidly, quickly arriving almost to the same volume fraction. The progressive transformation of χ to σ, occurring mainly after 80 min., has been noted (Figure 8). The ferrite transformation is not complete.

After aging at 1,000ºC for 5 min., χ and σ have been detected mainly at grain boundaries, with a few inside the ferrite grains. The amount of each phase is about 0.5%. By increasing the time, the amount of χ slowly decreases while the amount of σ increases to its maximum value after 15 minutes. Heating times longer than 20 min. can be compared to a non-complete solubilization, with a partial dissolution of the phases, and chromium, molybdenum, and tungsten in solid solution. These data confirm that the 2507 grade must be solubilized at T>1,050º if the secondary phase free structure is mandatory.

Continuous Cooling of SAF 2205

The morphology of the phases after continuous cooling is very similar to that observed in the isothermal aging tests (the precipitation occurs at the α/γ grain boundaries and especially at the triple points), while the formation sequence of secondary phases seems to be quite different. The total amount of secondary phases is lower for the highest solubilization temperature, in agreement with Reference 16, and strongly depends both on the cooling rates and on the solubilization temperature. The critical cooling rate for σ-phase formation is 0.35ºC/s, when a σ content of 0.2% is obtained. When the cooling rate decreases the σ content gradually increases and, at about 0.1–0.15°C/s, small χ-phase particles appear. Therefore, the χ phase forms at lower cooling rates than the σ phase and 0.3ºC/s is the minimum cooling rate to satisfy the generally accepted toughness requirements.

CONCLUSION

In order to study the kinetics of phase formation and their effect on fracture mechanisms the right technique to detect secondary phases in duplex stainless steels is not always the traditional one, especially when low contents of intermetallic phases are desired.

References

1. J. Charles, *Proceedings of Duplex Stainless Steels '91* (Milano, Italy: Italian Association of Metallurgy, 1991), pp. 151–167.
2. J.O. Nilsson, *Materials Science and Technology* 8 (1992), pp. 685–700.
3. J.O. Nilsson, *Proc. 5th World Conference on Duplex Stainless Steel* (Zutphen, The Netherlands: KCI Publishing, 1997), pp. 73–82.
4. J.O. Nilsson et al., *Metallurgical and Materials Transaction A,* 27A (1996), pp. 2196–2208.
5. N. Lopez, M. Cid, and M. Piuggali, *Corrosion Science,* 41 (1991), pp. 1615–1631.
6. R.J. Johansen et al., *Proceedings of Duplex 2000* (Venezia, Italy: Italian Association of Metallurgy, 2000), pp. 405–414.
7. J. Dobranszky et al., *Spectrochimica Acta part B*, 59 (2004), pp. 1781–1788.
8. R.N. Gunn, *Proceedings of Duplex America 2000* (Zutphen, The Netherlands: KCI Publishing, 2000), pp. 299–305.
9. J. Erneman et al, *Material Science Technology,* 20 (2004), pp. 1245–1251.
10. M.A. Dominguez-Anguilar and R.C. Newman, *Corrosion Science,* 48 (2006), pp. 2560–2576.
11. J. Michalska and M. Sozanska, *Mater. Character.*, 56 (2006), pp. 355–362.
12. Y.H. Lee et al., *Material Science Technology,* 14 (1998), pp. 757–764.
13. I. Calliari, G. Straffelini, and E. Ramous, *Proceedings of international Conference on Duplex* (Grado, Italy: Italian Association of Metallurgy, 2007).
14. I. Calliari, E. Ramous, and M. Zanesco, *J. Materials Science,* 41 (2006), pp. 7643–7649.
15. I. Calliari, K. Brunelli, and E. Ramous, submitted to *Material Science and Technology*.
16. T.H. Chen and J.R. Yang, *Materials Science and Engineering,* A311 (2001), pp. 28–41.

I. Calliari, K. Brunelli, M. Dabalà, and E. Ramous are with the Department of Innovation in Mechanics and Management (DIMEG), University of Padova; via Marzolo 9, 35131 Padova, Italy. Prof. Calliari can be reached at irene.calliari@unipd.it.